Journal of The Electrochemical Society, **163** (1) A5244-A5252 (2016)
0013-4651/2016/163(1)/A5244/9/$33.00 © The Electrochemical Society

JES Focus Issue on Redox Flow Batteries—Reversible Fuel Cells

Modeling of Ion Crossover in Vanadium Redox Flow Batteries: A Computationally-Efficient Lumped Parameter Approach for Extended Cycling

Philipp A. Boettcher,[a] Ertan Agar,[b,*] C. R. Dennison,[c,d] and E. Caglan Kumbur[d,z]

[a]*Department of Mechanical Engineering and Mechanics, Drexel University, Philadelphia, Pennsylvania 19104, USA*
[b]*Electrochemical Energy Systems and Transport Laboratory, Department of Mechanical Engineering, University of Massachusetts Lowell, Lowell, Massachusetts 01854, USA*
[c]*Laboratoire d'Electrochimie Physique et Analytique, Ecole Polytechnique Federale de Lausanne-Valais Wallis, CH-1951 Sion, Switzerland*
[d]*Electrochemical Energy Systems Laboratory, Department of Mechanical Engineering and Mechanics, Drexel University, Philadelphia, Pennsylvania 19104, USA*

In this work, we have developed a zero-dimensional vanadium redox flow battery (VRFB) model which accounts for all modes of vanadium crossover and enables prediction of long-term performance of the system in a computationally-efficient manner. Using this model, the effects of membrane thickness on a 1000-cycle operation of a VRFB system have been investigated. It was observed that utilizing a thicker membrane significantly reduces the rate of capacity fade over time (up to ∼15%) at the expense of reducing the energy efficiency (up to ∼2%) due to increased ohmic losses. During extended cycling, the capacity of each simulated case was observed to approach an asymptote of ∼60% relative capacity, as the concentrations in each half-cell reach a quasi-equilibrium state. Simulations also indicated that peak power density and limiting current density exhibit a similar asymptotic trend during extended cycling (i.e., an ∼10–15% decrease in the peak power density and an ∼20–25% decrease in the limiting current density is observed as quasi-equilibrium state is reached).

Manuscript submitted July 28, 2015; revised manuscript received November 4, 2015. Published December 1, 2015. *This paper is part of the JES Focus Issue on Redox Flow Batteries–Reversible Fuel Cells.*

Recently, vanadium redox flow batteries (VRFBs) have gained significant interest as one of the most promising electrochemical systems for grid-scale energy storage due to their several advantages over conventional batteries.[1,2] Among these advantages, the most important ones are their ability to decouple power and energy rating due to their unique system architecture, and their flexible design.[3–6] Despite these advantages, one major challenge which hinders their commercial viability is the relatively higher capital cost of these systems.[5] According to a recent study by Pacific Northwest National Laboratory, the current capital cost of a VRFB system is about $350 per kWh for 4-h application,[7] which is much higher than the capital cost target set by government agencies. The current capital cost target of The Department of Energy's Office of Electricity Delivery and Energy Reliability is $250 per kWh, falling to $150 per kWh in the future for a 4-hour energy storage system.[8]

One possible approach to reduce the capital cost is to improve the performance of these systems for less material use. To date, the majority of research has focused on improving the performance of individual components, such as developing high power density electrodes[4,9–16] and exploring high energy capacity electrolytes.[17–21] In line with these studies, another approach to reduce the capital cost is to increase the lifetime of VRFB systems. Currently, the lifetime of these systems is limited by the capacity fade during cycling, which is primarily governed by unwanted active species transport across the membrane (i.e., species crossover).[22] Developing sophisticated mathematical models to mimic the VRFB operation is imperative to investigate the capacity fade and related performance losses in these systems due to lengthy time requirements and practical limitations of experimental cycling analysis. So far, there are several studies reported that have focused on investigating the change in long-term performance of VRFBs based on vanadium crossover across the membrane.[22–29] The early attempts were made by Syllas-Kazacos and her co-workers. They developed a zero-dimensional, transient model including vanadium diffusion across the membrane to predict the energy capacity during cycling.[23,24] The main goal in this study was to determine when electrolyte rebalancing should take place to restore the lost capacity as a result of vanadium diffusion across the membrane. Recently, they have extended this model to incorporate the effects of temperature and bulk electrolyte transport in addition to vanadium diffusion across the membrane on capacity fade during cycling.[25]

With a similar objective, our group at Drexel has developed an experimentally-validated, two-dimensional, transient model which incorporates the transport of vanadium species as a result of three different transport modes (diffusion, convection, and migration).[22] Using this model, the effects of each species transport mechanism on crossover and capacity fade were investigated. Accordingly, several strategies to mitigate the capacity fade have been proposed, such as tailoring membrane properties[26] and running VRFB under constant pressure[27] or asymmetric current density[28] mode depending on the membrane properties. In general, these studies have revealed that each of three species transport mechanisms has important implications on the species crossover. Depending on the chemical structure of the membrane and operating conditions, they make different contributions to the crossover and resulting capacity fade. However, the computational complexity of this model hinders its implementation to predict lifetime of VRFB. More specifically, this model could not be used to investigate VRFB performance during extended cycling operation (e.g., for 1000 cycles and more) due to its lengthy processing requirement similar to experimental cycling analysis.

With this motivation, in this study we introduce a computationally-efficient lumped parameter modeling approach to predict the long-term performance of a VRFB. Using this approach, we have developed a zero-dimensional performance model that captures the key physics necessary to determine the capacity fade and enables extended cycling of a VRFB in a computationally efficient manner (∼75× more efficient compared to our previous 2-D modeling approach[22,26–28] due to the reduced dimensionality). A detailed validation study has been performed to assess the features and capabilities of this new modeling approach. With the help of significantly shorter simulation time for a complete cycle (∼2 minutes using a laptop with 2.66 GHz Intel Core i7 processor and 4GB RAM memory for a cycle between 1.1–1.7 V at 50 mA cm^{-2}), a 1000-cycle operation has been simulated as a case study in order to investigate the effects of membrane thickness on long-term performance, and the results are presented.

*Electrochemical Society Active Member.
[z]E-mail: eck32@drexel.edu

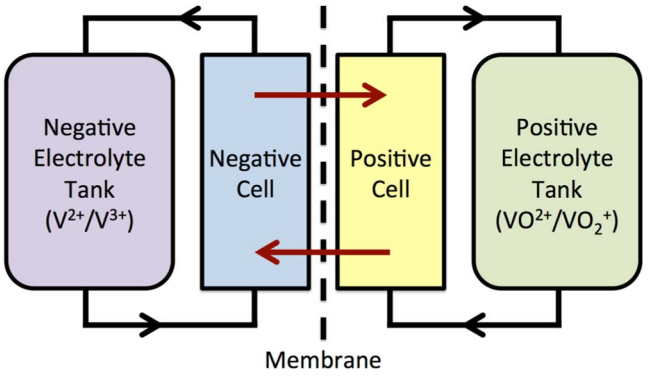

Figure 1. Schematic of the modeled VRFB domains.

Model Formulation

The VRFB is modeled as four coupled elements: the negative half-cell, the positive half-cell, the negative electrolyte tank, and the positive electrolyte tank (see Fig. 1). The model is created with the following assumptions and governing equations.

Assumptions.— The model is based on the following assumptions:

1. All quantities are assumed to be homogeneous in each element.
2. The positive electrolyte tank is only coupled to the positive half-cell.
3. The negative electrolyte tank is only coupled to the negative half-cell.
4. The positive and negative half-cells are coupled via the membrane.
5. The electrodes on both half-cells are identical.
6. All elements are isothermal.
7. All reactions occur instantaneously.
8. The dilute solution approximation is utilized for species transport.
9. Hydrogen and oxygen evolution reactions are neglected.

Governing equations.— The underlying chemical redox reactions occurring in the negative and positive half-cell are as follows:[1,2]

$$V^{3+} + e^- \underset{\text{discharge}}{\overset{\text{charge}}{\rightleftharpoons}} V^{2+} \qquad \text{(Negative)} \qquad [1]$$

$$VO^{2+} + H_2O \underset{\text{discharge}}{\overset{\text{charge}}{\rightleftharpoons}} VO_2^+ + e^- + 2H^+ \qquad \text{(Positive)} \qquad [2]$$

where VO^{2+} and $VO^+{}_2$ are the V^{4+} and V^{5+} oxidation states, respectively.

The flow of the electrolyte through the porous electrode is calculated from the mass conservation equation assuming that the electrolytes are incompressible and the velocity is spatially uniform. For each species i, the mass conservation equation for each half-cell is given by:

$$\frac{d}{dt}\left(\varepsilon c_i^c\right) + \frac{d}{dt}N_i = -S_i \qquad [3]$$

where ε is the porosity, c_i^c is the concentration in the cell, c, N_i is the flux and S_i is the source term. The flux term can be separated into in-flow from and out-flow to the tank and the convection, diffusion, and migration across the membrane. The flux to and from the tank, t, is given by:

$$N_i^t = \left(c_i^t - c_i^c\right)\frac{\omega}{A_{hydraulic}} \qquad [4]$$

where, c_i^t is the concentration in the tank, t, ω is the volumetric flow rate and $A_{hydraulic}$ is the hydraulic cross sectional area of the half-cell that the flow experiences. Through the membrane, m, the diffusion, migration, and convection are described by the Nernst-Planck equation:

$$N_i^m = -D_i^m\frac{\left(c_{i,neg}^m - c_{i,pos}^m\right)}{\delta_{diff}} - z_i\frac{D_i^m}{RT}c_i F\frac{\left(\phi_{neg}^m - \phi_{pos}^m\right)}{\delta_{diff}} + v^m c_i \qquad [5]$$

where z_i is the valence for species i, R is the universal gas constant and T is temperature, F is the Faraday constant, ϕ^m is the liquid potential, and v is the velocity. Diffusivities for all species across the membrane, D_i^m, are given in Table I. The species gradient across the membrane are calculated by considering that a boundary layer develops in each half-cell on both sides of the membrane limiting mixing, and the diffusion distance δ_{diff} is

$$\delta_{diff} = t_{mem} + 2\delta_{BL} \qquad [6]$$

The membrane thickness, t_{mem}, is varied in this study and the boundary layer thickness, δ_{BL}, is held constant at 100 μm.[22] In this formulation of the migration term, the dilute solution approximation is used and thus the ionic mobility in the electrolyte, is represented using the Nernst- Einstein equation:[34]

$$u_i^m = \frac{D_i^m}{RT} \qquad [7]$$

The liquid potential drop across the membrane is also assumed to occur over the diffusion distance and is calculated from Ohm's law:

$$\phi_{neg}^m - \phi_{pos}^m = \frac{I}{\sigma_{eff}^m}\frac{\delta_{diff}}{A_{cross}} \qquad [8]$$

where I is the current, A_{cross} is the cell cross sectional area, and σ_{eff}^m is the effective conductivity of the membrane:

$$\sigma_{eff}^m = \frac{F^2}{RT}\sum_i z_i^2 D_i^m c_i^m \qquad [9]$$

where c_i^m is calculated by taking the arithmetic mean of the positive and negative half-cell.

The convection velocity across the membrane is calculated from an alternate form of Schlogl's equation:[35]

$$v^m = -\frac{\kappa_p}{\mu_w}\left(p_{neg} - p_{pos}\right) - \frac{\kappa_\varphi}{\mu_w}c_f F\left(\phi_{neg}^m - \phi_{pos}^m + \nabla\phi_{diff}^m\right) \qquad [10]$$

where κ_p is the hydraulic permeability, μ_w is the viscosity of water, $(p_{neg} - p_{pos})$ is the pressure gradient across the membrane, κ_φ is the electrokinetic permeability, and c_f is the fixed acid concentration. Schlogl's equation accounts for osmosis and electro-osmosis. The pressure gradient between the two half-cells drives the osmotic flux of water through the membrane. The electro-osmotic convection is in turn captured by the second term as discussed in Refs. 22,36, where the effective diffusion potential gradient, $\nabla\phi_{diff}^m$ is calculated by

$$\nabla\phi_{diff}^m = \frac{F}{\sigma_{eff}^m}\sum_i z_i D_i^m\left(c_{i,neg}^m - c_{i,pos}^m\right) \qquad [11]$$

Table I. Membrane properties and parameters for Nafion 117.

Property/Unit	Value
Membrane conductiviy (S m^{-1})	10
Membrane Thickness (m)	2.03×10^{-4}
Fixed acid concentration (mol m^{-3})	1431
Electrokinetic permeability (m^2)[a]	1.13×10^{-20}
Hydraulic permeability (m^2)	1.58×10^{-18}[30]
V^{2+} membrane diffusion coefficient (m^2 s^{-1})[a]	6.25×10^{-12}
V^{3+} membrane diffusion coefficient (m^2 s^{-1})	5.93×10^{-12}[31]
V^{4+} membrane diffusion coefficient (m^2 s^{-1})	5.0×10^{-12}[31]
V^{5+} membrane diffusion coefficient (m^2 s^{-1})	1.17×10^{-12}[31]
H^+ membrane diffusion coefficient (m^2 s^{-1})	3.35×10^{-9}[32]
HSO_4^- membrane diffusion coefficient (m^2 s^{-1})	4×10^{-11}[33]

[a]Fitted parameter

Table II. Electrode dimensions and properties.

Property/Unit	Value
Electrode height (m)	0.035
Electrode width (m)	0.0285
Electrode thickness (m)	0.004
Hydraulic cross sectional area – $A_{hydraulic}$ (m^2)	1.12×10^{-4}
Cell cross sectional area – A_{cross} (m^2)	0.001
Electrode specific surface area (m^{-1})	35000
Cozeny-Karman coefficient	180[37]
Electrode porosity	0.93[22]
Mean pore radius (μm)	50.3[22]

In Schlogl's equation the pressure difference, $(p_{neg} - p_{pos})$, is calculated from Darcy's law in which the effective permeability is determined from the Kozeny-Carman equation:

$$(p_{neg} - p_{pos}) = \frac{\omega L}{A_{cross}} \frac{C_{KC}}{4r_p^2} \frac{(1-\varepsilon)^2}{\varepsilon^2} \Delta\mu \quad [12]$$

where L is the cell length, C_{KC} is the Kozeny-Carman constant,[37] r_p is the mean radius of the electrode pores, and $\Delta\mu$ is the difference in dynamic viscosity between the electrolytes. All the electrode properties are given in Table II. Also, it's important to note that the viscosity values are assumed to be constant.[22] The main source for change in vanadium concentrations is the applied or drawn current. The source terms are specified in each half cell individually, giving the source terms for V(II) and V(III) in negative half-cell as

$$S_{II} = -\frac{i}{F};\ S_{III} = \frac{i}{F} \quad [13]$$

and the source terms for V(IV) and V(V) in the positive half-cell as

$$S_{IV} = \frac{i}{F};\ S_V = -\frac{i}{F} \quad [14]$$

where i is the current density in [A/m^3]. In addition, the crossover of species contributes to the source and sink term, which are independent of the current. The crossover of vanadium leads to the following side reactions:[38]

Negative electrolyte:

$$VO^{2+} + V^{2+} + 2H^+ \rightarrow 2V^{3+} + H_2O \quad [15]$$

$$VO_2^+ + 2V^{2+} + 4H^+ \rightarrow 3V^{3+} + 2H_2O \quad [16]$$

Positive electrolyte:

$$V^{2+} + 2VO_2^+ + 2H^+ \rightarrow 3VO^{2+} + H_2O \quad [17]$$

$$V^{3+} + VO_2^+ \rightarrow 2VO^{2+} \quad [18]$$

In this model, it is assumed that these side reactions occur instantaneously once the species has crossed into the main flow of the half-cell. Once the concentration in each half-cell has been established in each time step, the cell voltage, E_{cell}, can be obtained by calculating the open circuit voltage, E_0, using the Nernst equation, the overpotential, η using the Butler-Volmer equation, as well as the voltage to overcome each half-cell resistance, $R_{half\text{-}cell}$.

$$E_{cell} = E_{0,+} - E_{o,-} - (\eta_+ - \eta_-) - I R_{cell} \quad [19]$$

The Nernst Equation gives the open circuit voltage for each half-cell, $E_{(0,+/-)}$.

$$E_{0,-} = E'_{0,-} + \frac{RT}{F} \ln\left(\frac{c_{III}}{c_{II}}\right) \quad \text{(Negative)} \quad [20]$$

$$E_{0,+} = E'_{0,+} + \frac{RT}{F} \ln\left(\frac{c_V \cdot (c_{H^+})^2}{c_{IV}}\right) \quad \text{(Positive)} \quad [21]$$

where $E'_{(0,+/-)}$ is the standard reduction potentials. The overpotential is calculated from the Butler-Volmer equation expressed in the following form assuming that the surface and electrolyte concentrations are the same.[22]

$$i_i = \alpha F k_-(c_{II})^{(1-\alpha_-)}(c_{III})^{\alpha_-} \times \left[\exp\left(\frac{(1-\alpha_-)F\eta_-}{RT}\right) - \exp\left(\frac{-\alpha_- F\eta_-}{RT}\right)\right] \quad [22]$$

$$i_i = \alpha F k_+(c_{IV})^{(1-\alpha_+)}(c_V)^{\alpha_+} \times \left[\exp\left(\frac{(1-\alpha_+)F\eta_+}{RT}\right) - \exp\left(\frac{-\alpha_+ F\eta_+}{RT}\right)\right] \quad [23]$$

The total cell resistance is calculated by adding the membrane resistance to the electrode resistance (assumed to be constant at 0.2 Ω cm^2). The membrane conductivity was estimated to be 10 S/m.[39]

$$R_{cell} = 2R_{electrode} + \frac{t_{mem}}{A_{mem}\sigma_{mem}} \quad [24]$$

It's important to note that in addition to the electrokinetic permeability of the membrane (κ_φ) and the diffusivity of V^{2+} across the membrane (D_{II}^m), the reaction rate constants ($k_{+,-}$) and the charge transfer coefficients ($\alpha_{+,-}$) are also used as fitting parameters as stated in our group's earlier paper.[22] Among these, only the diffusivity of V^{2+} across the membrane is changed compared to the previous study in order to achieve closer agreement for the ionic transport through the membrane and to compensate the dimensional limitations of this model. More detailed information about the model including governing equations, initial and boundary conditions, and constant parameters can be found in our group's earlier studies.[22,26,28]

Model Validation

Cyclic performance comparison.— As a first step in validating the predictions of this simplified 0-D model, the predicted cell voltage during a single charge/discharge cycle at 50 mA cm^{-2} constant current density operation was compared with our previous 2-D model predictions, as well as experimental data obtained under similar testing conditions by Kim et al.[40] A comparison of these data sets is shown in Fig. 2a. Very good agreement was found between the 0-D model and the experimental data, with only 5.0% and 4.2% average error in voltage for the charge and discharge cycles, respectively. For comparison, the 2-D model exhibited 1.8% and 1.9% average error during charging and discharging, respectively.[22] The relatively minor increase in error associated with the 0-D model is quite acceptable given its simplified formulation and much greater computational efficiency. Subsequently, the long-term capacity fade predicted by the 0-D model was compared with the predictions of our previous 2-D model, and the experimental results of Kim et al.[40] (Fig. 2b). The 0-D model was found to exhibit 5.0% average error with respect to the experimental data, as compared to 4.2% average error for the 2-D model for 45 cycles.[22] It should be noted that cycles 7 through 10 were excluded from the error calculations, due to anomalies in the experimental data. The good agreement between the simplified 0-D model and the experimental data provides a high level of confidence in the predictive capabilities of the model formulation.

To further compare the predictive capability of the 0-D model versus the 2-D model, charge/discharge data for specific cycles was compared. This comparison illustrates the coupling between concentration changes due to crossover and the electrochemical performance of the cell. As seen in Fig. 3a, at cycle 10, the 0-D and 2-D models are in good agreement. As cycling continues, the 0-D model is observed to predict acceptable cycle times (~17% at cycle 40, Fig. 3d), considering the significant difference in dimensionality and resolution between two models.

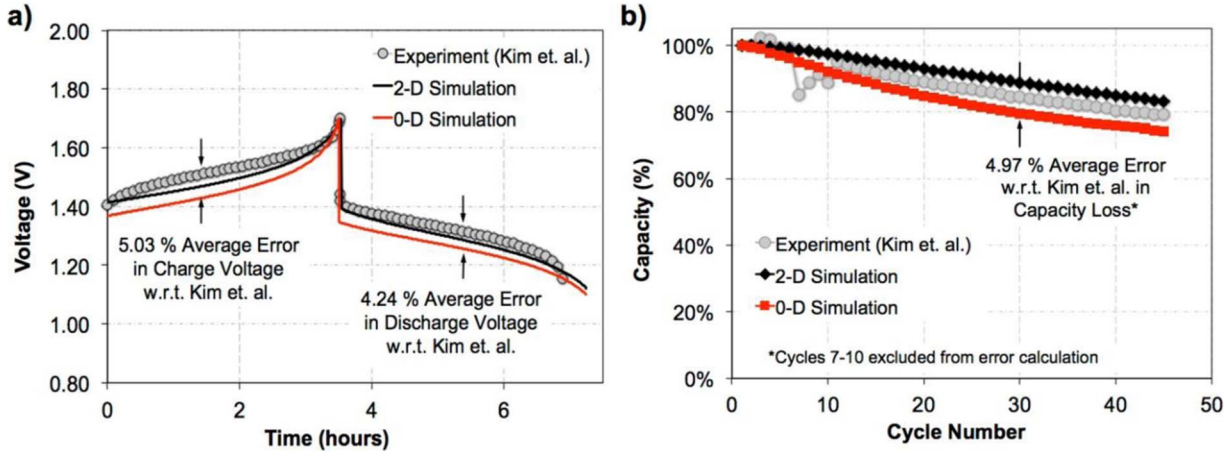

Figure 2. Comparison of a) single cycle voltage and b) long-term capacity fade for the proposed 0-D model, our previous 2-D model, and experimental 45-cycle data by Kim et al.[40] (a 10-cm^2 VRFB cell operated at a 20 mL min^{-1} electrolyte flow rate and a 50 mA cm^{-2} constant current density).

Comparison of species crossover.— In order to further compare the crossover and capacity fade predictions of the simplified 0-D model with the 2-D model, the concentration (Fig. 4) and flux (Fig. 5) values were investigated. In Fig. 4, it was observed that the concentration change in the 0-D model is larger than the 2-D model predictions, particularly for the V^{3+} and V^{4+} species. This apparent discrepancy may be partially explained by the results presented in Fig. 5. When considering the flux values, it was found that 0-D model consistently predicts higher fluxes than the 2-D model, with the exception of the V^{5+} species. These higher flux values may be due to the reduced spatial resolution which is inherent to the 0-D modeling approach. Essentially, this simplified approach assumes a uniform concentration across the entire surface of the membrane, whereas the 2-D framework allows for spatial concentration gradients across the surface of the membrane (e.g., during discharging, V^{2+} and V^{5+} are expected to be high near the inlet, and deplete as electrolyte flows toward the outlet). As a result of this simplification, the 0-D model may predict higher concentrations of certain species adjacent to the membrane, resulting in larger flux values.

Another limitation of the 0-D modeling approach is the assumption of uni-directional flux of each active species from its native compartment to the opposing compartment. In the 2-D model, a finite amount of time is required for species to cross the thickness of the membrane, from one half-cell to the other. In this way, the membrane acts a reservoir where all four species of vanadium exist simultaneously, allowing species flux in both directions. However, due to the

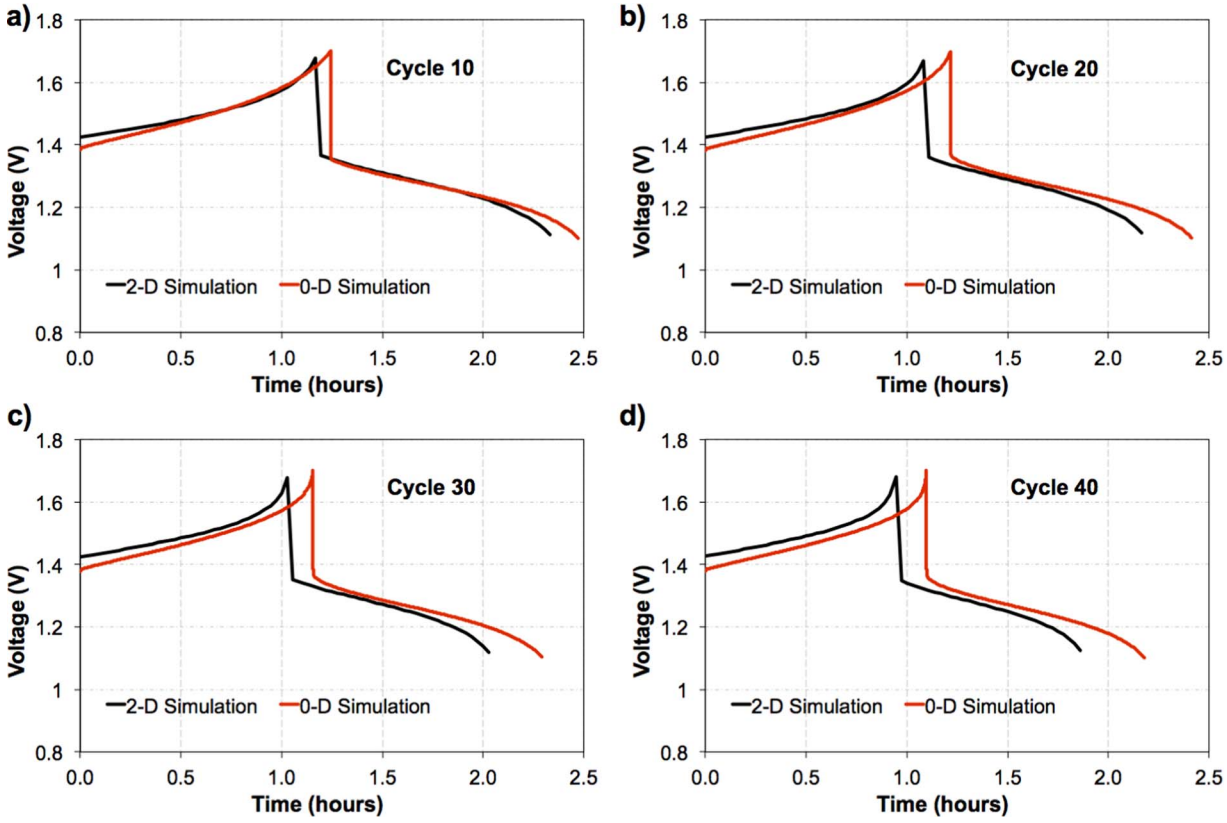

Figure 3. Comparison of voltage predictions for various cycles: a) Cycle 10, b) Cycle 20, c) Cycle 30, d) Cycle 40.

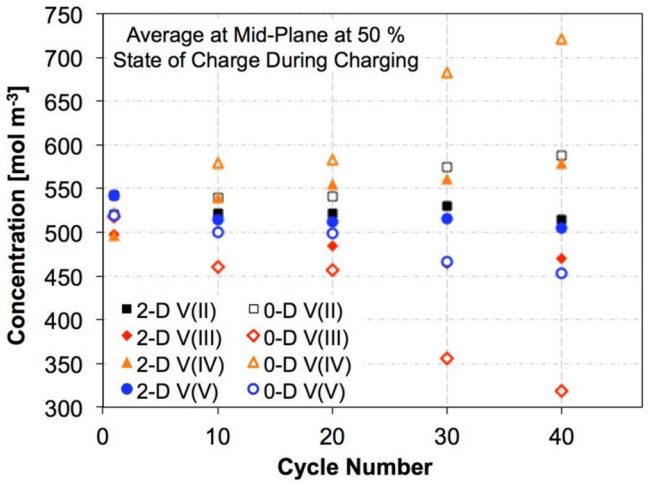

Figure 4. Comparison of concentration changes during cycling.

simplifications of the 0-D approach employed here, species are assumed to cross the membrane instantaneously, and are immediately consumed by the side-reactions in the adjacent compartment. In this way, an implicit assumption of the 0-D model is that only native vanadium species may exist in their respective half-cell (e.g., V^{2+} V^{3+} in the negative half-cell, and V^{4+}/V^{5+} in the positive half-cell). As a result, it is not possible to have a flux of a species toward its native half-cell (e.g., a flux of V^{2+} into the negative half-cell), because there is no source for that species on the opposite side of the membrane. This is the reason why, for example, the 0-D model predicts zero flux of V^{4+} due to migration during discharging in Fig. 5c, while the 2-D model predicts a small flux toward the positive half-cell.

Despite these limitations, the 0-D model was still shown to provide a good predictive capability of both charge/discharge behavior and relative capacity. Accurate prediction of both of these factors is essential for developing full scale VRFB systems and understanding their long-term performance. Given the satisfactory performance of our computationally efficient model, we have investigated the role of membrane thickness on the long-term performance of these systems, which are discussed in the following sections.

Results and Discussion

Effects of membrane thickness.— A critical consideration in the engineering of full-scale RFB systems is the choice of membrane. It is well known that changing the thickness of the membrane makes it possible to tailor the crossover and resistive losses within the cell (e.g., thinner membranes exhibiting significantly higher rates of crossover while providing a decrease in ohmic resistance[6]). However, as the cell is cycled, crossover causes the concentrations in each half-cell to change, affecting both the capacity of the system, as well as the available power and current density. The long-term tradeoff between membrane thickness, capacity fade, and performance characteristics of the system is not well understood. As a first step to these long-term tradeoffs, several common membrane thicknesses ranging from 25.4 to 254 μm (1 to 10 mils) were simulated. Figure 6 shows the change in relative capacity during cycling for these membranes.

As seen in Fig. 6, the initial increase in capacity is observed as a result of the initial conditions chosen and the voltage limits used,[29] whereas at higher cycle numbers the effect of membrane thickness is more clear. At cycle 100, the cell with the thickest membrane (254 μm) retains 86% of its initial capacity, while the thinnest membrane (25.4 μm) only retains 71% capacity. While the difference in relative capacity after 100 cycles is only 15% or less for the membranes tested, the lower rate of capacity fade observed for thicker membranes means these systems would need less frequent mainte-

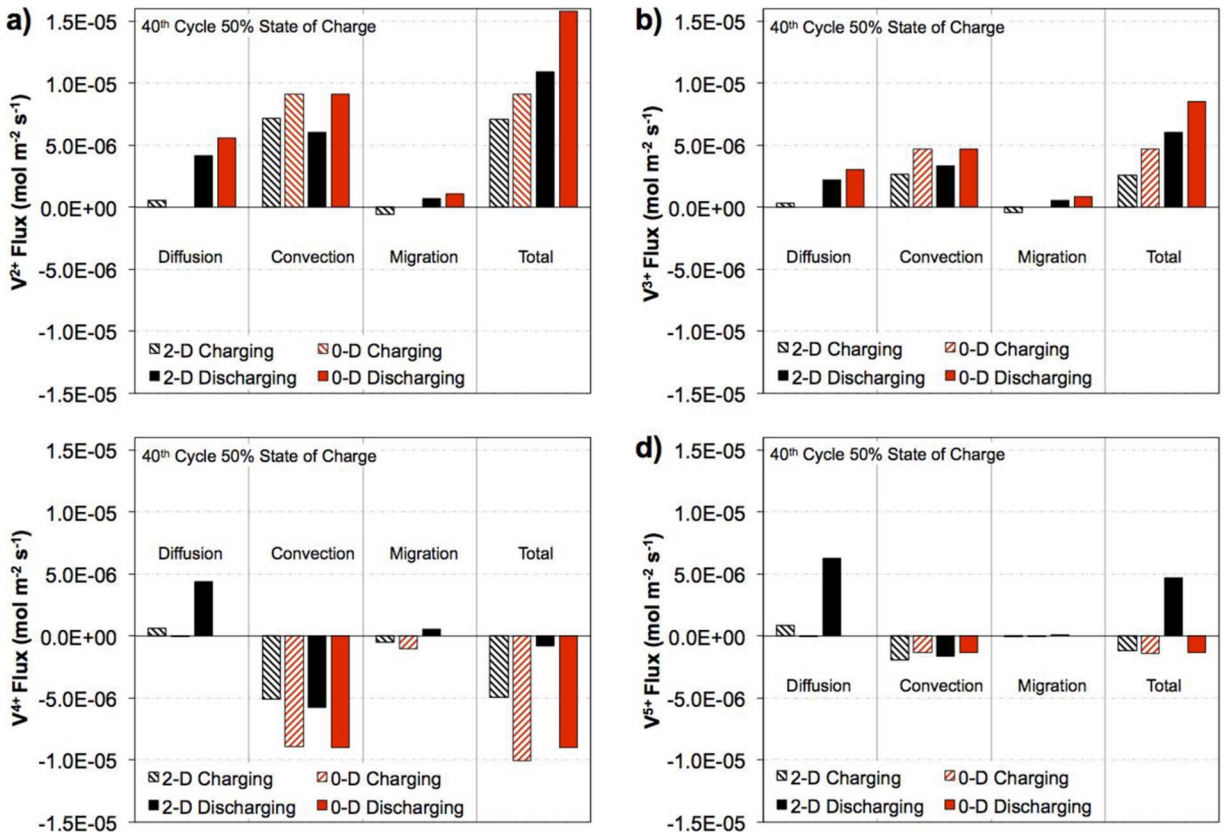

Figure 5. Comparison of fluxes for various species: a) V^{2+}, b) V^{3+}, c) V^{4+}, d) V^{5+}.

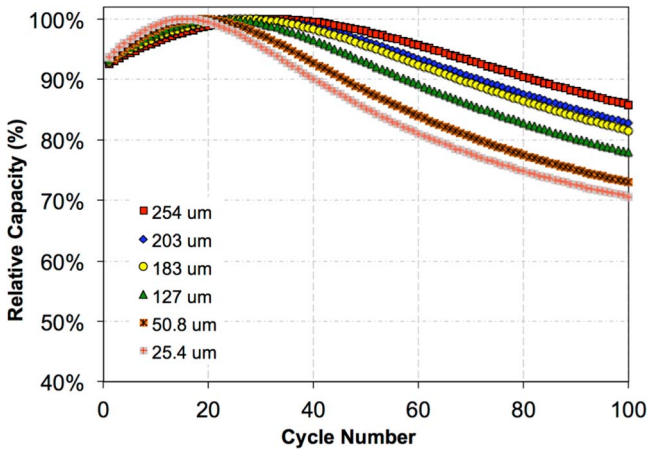

Figure 6. Relative capacity change during cycling for membranes of varying thickness, from 25.4 μm to 254 μm.

nance. For example, if a VRFB installation is typically serviced when the relative capacity decays to 70%, then the system with a 25.4 μm thick membrane would require service at ∼100 cycles, while a system with a 254 μm thick membrane may continue to operate for 60+ additional cycles. This deferral of maintenance could significantly reduce operating costs for full-scale installations.

Beyond capacity fade, the efficiency of the system will also impact the operating costs of VRFB installations. Fig. 7a shows the effect of cycling on coulombic, voltage, and energy efficiency for a cell utilizing a 203 μm thick membrane. The coulombic efficiency remains relatively constant (∼99%) throughout cycling. Conversely, the voltage efficiency actually increases as cycling progresses, changing from 83.5% to 86.0%. The energy efficiency exhibits an increasing trend, similar to the voltage efficiency.

Figures 7b–7d show the efficiencies of each membrane thickness at selected cycles. For the 10th cycle (Figure 3b), the 25.4 μm thick membrane exhibits the lowest coulombic efficiency of 98.3%, while the thickest membrane (254 μm) exhibits marginally higher coulombic efficiency of 99.0%. As expected from Figure 6a, the coulombic efficiency is relatively constant during cycling. The thinnest membrane exhibited a voltage efficiency of 85.2% at cycle 10, which steadily rose to 87.4% by cycle 100. The thickest membrane exhibited slightly lower voltage efficiency values of 83.5% and 85.6% at cycles 10 and 100, respectively. The intermediate-thickness membranes exhibited efficiencies between those of the thickest and thinnest membranes. The reduced voltage efficiency observed for the thicker membranes is expected, due to the increased ionic path-length within the membrane which results in increased Ohmic losses during operation. Similar to capacity fade, the system efficiency plays a critical role in determining the operating costs for a full-scale VRFB installation.

Cycling stability.— To further project the operating behavior of the system, while exploiting the computational efficiency of the model, we simulated 1000 cycles for a system based on a 203 μm thick membrane. The change in relative capacity during cycling is shown in Figure 8a. After ∼500 cycles, the system reaches an asymptote at ∼64.2% relative capacity, indicating that the system has reached a quasi-equilibrium state. This suggests that as cycling proceeds, crossover causes the concentrations of active species in each half-cell to approach a steady state. Thus, the exact relative capacity at which this asymptote occurs will depend strongly on the initial concentrations of the reactants as well as the transport properties of the membrane. It is likely that the location of the asymptote also depends

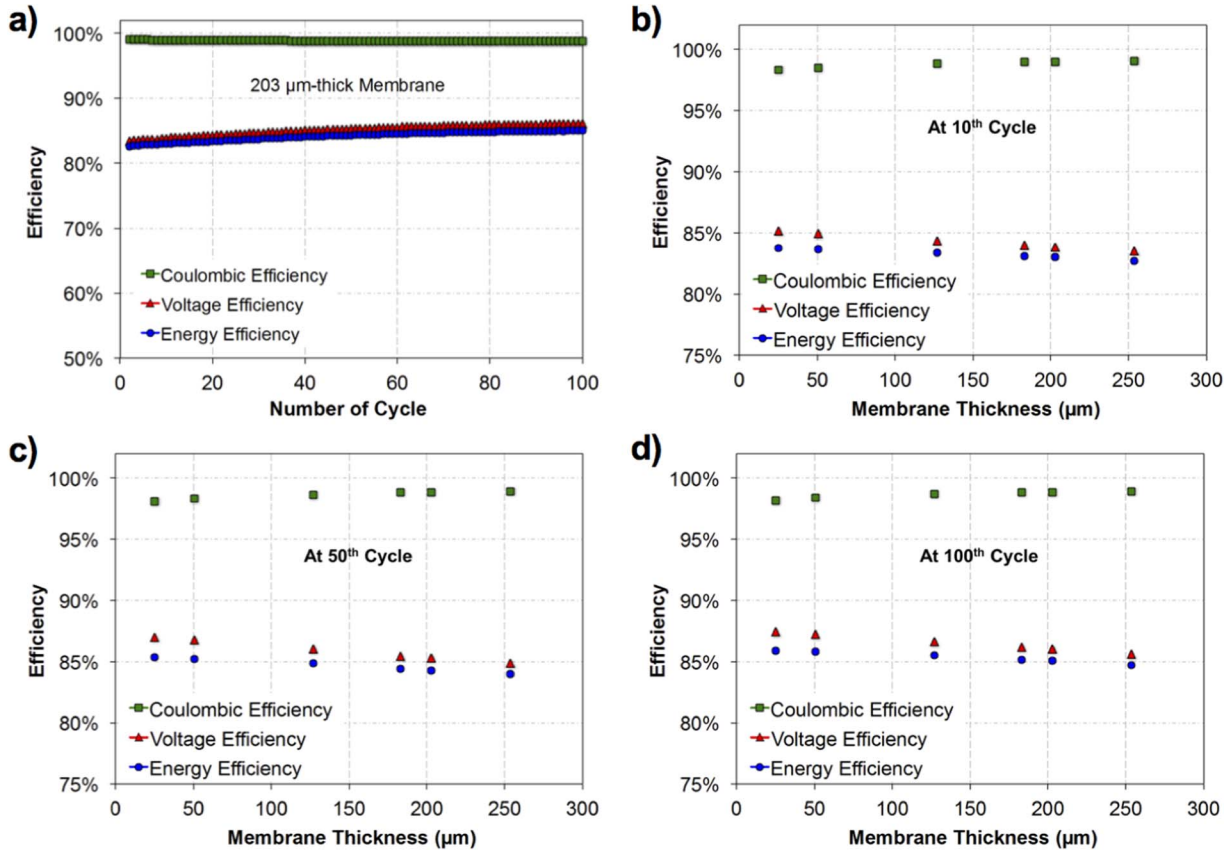

Figure 7. a) Coulombic, voltage, and energy efficiency as a function of cycle number for the 203 μm thick membrane. Efficiencies for different membrane thicknesses after b) 10, c) 50, and d) 100 cycles.

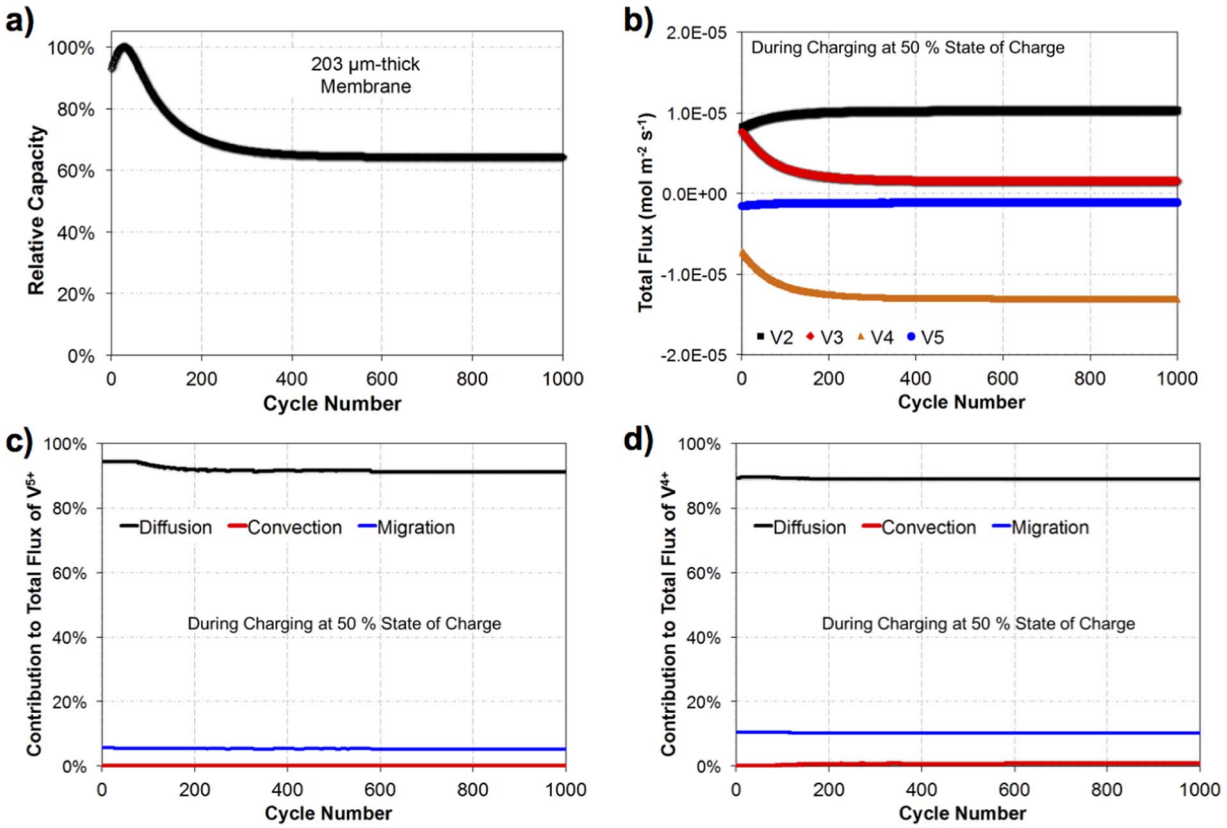

Figure 8. a) Relative capacity fade over 1000 cycles for a cell utilizing a 203 µm membrane. b) Total flux of each vanadium species at 50% state of charge during the charge cycle. The relative contribution of diffusion, convection, and migration for the c) $V3^+$ and d) $V4^+$ species.

on the cycle parameters (e.g., min/max voltage, current density, etc.) and mode of operation (e.g., voltage or concentration cutoff limit).

Figure 8b shows the total flux of each vanadium species during cycling. As cycling proceeds, the flux of each species varies until the system reaches quasi-equilibrium, as in Fig. 8a. Figures 8c-8d show the relative contributions of diffusion, convection, and migration to the total flux of V^{5+} and V^{4+} during charging. As expected from previous studies,[26,28] the transport in this system is dominated by diffusion. This diffusion dominance is believed to contribute to the asymptotic behavior seen in Figure 8a. It is possible that membranes which are convection-dominated may not exhibit such an asymptote, since the pressure and potential gradients between the two half-cells are not expected to change significantly as cycling progresses. For this reason, it is very important to understand the dominant transport mechanisms driving crossover in a given membrane in order to predict the long-term cycling stability of a system.

Polarization curve performance.— The shifting species concentrations which give rise to the asymptotic capacity decay seen in the previous section are also expected to impact the performance characteristics of the system. To explore these effects, we performed polarization curve simulations at every 20th cycle for 1000 cycles for different membrane thicknesses. Figures 9a–9b show exemplary polarization curves at the 20th and 500th cycle, respectively. In Figure 9a, the effect of membrane resistance results in slightly different slope at intermediate current densities. As a result, cells with thinner membranes exhibit higher peak power densities (<256 mW/cm^2) than cells with thicker membranes (>233 mW/cm^2). Each membrane reaches the same limiting current density (i.e., 350 mA/cm^2). However, after 500 cycles have elapsed, the peak power density has dropped significantly to 217 mW/cm^2 (~15% decrease) and 208 mW/cm^2 (~11% decrease) for the 25.4 and 254 µm thick membranes, respectively. This decrease can be seen in Figure 9c. Similarly, Figure 9d shows the decrease of limiting current density as cycling progresses. After 1000 cycles, the 254 µm case exhibits a limiting current density of 280 mA/cm^2, a 20% decrease versus the 20th cycle. The 25.4 µm case exhibits an even larger decrease of 26% (260 mA/ cm^2) over the same period. These changes in cell performance further highlight the effects that crossover can have on the long-term performance of a VRFB installation.

It's important to note that the localized mass transport effects within the porous electrode cannot be captured due to the dimensional limitations of this model. Thus, the limiting current observed in these polarization curves is largely due to significant depletion of the reactants passing through the cell, which causes a decrease in the Nernst potential. Furthermore, the irregularities seen in Figures 9c and 9d are artifacts resulting from the fact that the polarization curves are not simulated as a continuous sweep of current. Rather, the polarization behavior of the system was simulated in a manner similar to the real world experiments: the current was increased stepwise in increments of 10 mA/cm^2, each simulated for 30 seconds of model time. At the conclusion of each step, the final point (voltage, current density, power density) was taken for the polarization curve, before again incrementing the current. A cutoff voltage of 0.2 V was used to terminate the polarization curve simulation – if the simulated potential decreased below 0.2 V during the simulation time, then the polarization routine was ended. The data from the final incomplete step was discarded, as the cell could not maintain an acceptable voltage at that current density.

Discussion and outlook.— Using the current lumped parameter model, we were able to investigate the long-term performance of a VRFB in terms of crossover and related capacity fade. A non-zero asymptotic decay of relative capacity, peak power density, and limiting current density was observed for all cases examined in this work. These observations suggest that although significant changes

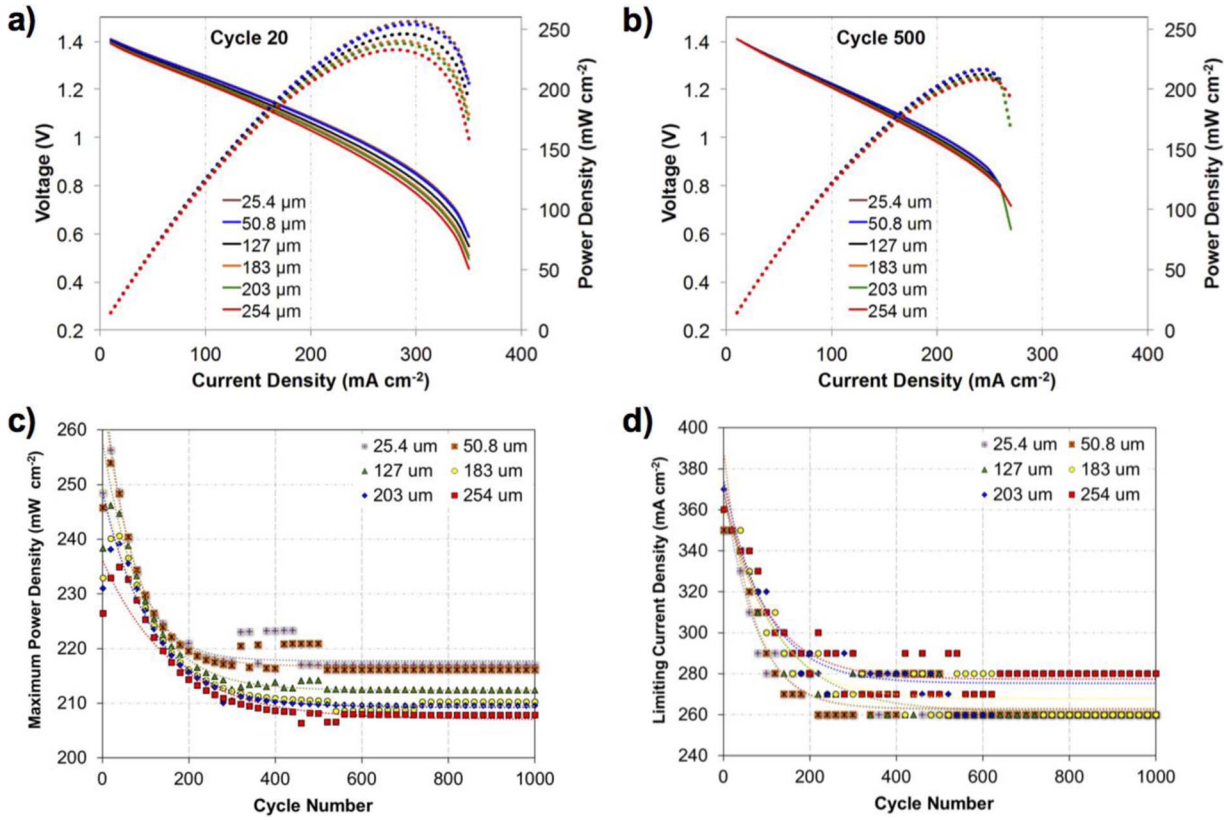

Figure 9. Simulated polarization curves for different membrane thicknesses at a) cycle 20, and b) cycle 500. Change in the c) maximum power density and d) limiting current density over 1000 cycles.

in system capacity and performance can occur during the first several hundred cycles, in lieu of proper maintenance a VRFB installation may actually be operated with degraded performance for many thousands of cycles after without further loss of performance. Of course, the model formulation described here does not account for degradation of individual cell components, which will impact the long-term operation of a VRFB.

Additionally, the case study presented here suggests that beginning-of-life performance characterization (e.g., capacity, peak power density, limiting current density) may significantly overpredict the long-term capabilities of the system. Using the model formulation presented here, it is possible to predict the long-term concentration changes occurring due to crossover which give rise to the changes observed here. Using these concentrations, simulated aged electrolytes could be prepared and used to characterize the performance of a cell setup. This simulated aging should provide a reasonable approximation of the middle-of-life performance characteristics of the system.

It is important to note that these simulations were performed assuming galvanostatic charge/discharge with potential limits. Full-scale flow battery installations may be subject to more dynamic loading conditions, with occasional idle periods. Although the case study presented here focuses on a simplified operating regime, the model formulation is readily adaptable to simulate more complex operation.

The trade-off between membrane conductivity and undesirable crossover of vanadium has often been managed by varying the thickness of the membrane to achieve the desired balancefor a given application. This model framework provides the capability to compare the long-term capacity and performance characteristics as a function of membrane thickness. These predictions will enable better design and engineering of flow battery systems for specific applications.

Conclusions

In this work, we have developed a zero-dimensional VRFB performance model which accounts for the different modes of vanadium transport across the membrane, and enables prediction of the long-term performance of the system in a computationally-efficient manner. This new model is built on a similar analytical framework to our previous 2-D crossover model, but is significantly more computationally-efficient ($\sim$75$\times$ reduction in computational time due to the reduced dimensionality). This modeling framework was shown to provide good agreement with long-term experimental cycling data. Accordingly, it was used to investigate the effects of membrane thickness on a 1000-cycle operation of a VRFB system.

Simulations indicate that utilizing a thicker membrane significantly reduces the rate of capacity fade during cycling at the expense of reducing the energy efficiency (up to 2%) due to increased ohmic losses. Over time, the capacity of each of the systems was observed to approach an asymptote of $\sim$60% relative capacity, as the concentrations in each half-cell reach a quasi-equilibrium state. Thicker membranes resulted in a higher asymptotic relative capacity. Polarization curve simulations revealed that peak power density and limiting current density exhibit a similar asymptotic trend during extended cycling. However, in this case thinner membranes were associated with higher cell performance. These results suggest that crossover in VRFBs is a self- limiting process which causes diminished system capacity and performance due to concentration changes in the two halves of the system.

The modeling framework introduced in this work enables efficient simulation of the long-term behavior of VRFB systems, and can be used to investigate the effects of key system parameters on the lifetime of these systems. Insights gained from these studies can be used to guide the system design and optimization efforts.

Acknowledgments

Support from the National Science Foundation (grant #1351161) is acknowledged.

References

1. M. Skyllas Kazacos and F. Grossmith, *J. Electrochem. Soc.*, **134**, 2950 (1987).
2. M. Rychcik and M. Skyllas-Kazacos, *J. Power Sources*, **22**, 59 (1988).
3. C. Blanc, *PhD Thesis*, Ecole Polytechnique Federal De Lausanne (2009).
4. D. S. Aaron, Q. Liu, Z. Tang, G. M. Grim, A. B. Papandrew, A. Turhan, T. A. Zawodzinski, and M. M. Mench, *J. Power Source*, **206**, 450 (2012).
5. A. Weber, M. M. Mench, J. Meyers, and P. Ross, *J. Appl. Electrochem.*, **41**, 1137 (2011).
6. D. Chen, M. A. Hickner, E. Agar, and E. C. Kumbur, *J. Membr. Sci.*, **437**, 108 (2013).
7. A. Crawford, V. Viswanathan, D. Stephenson, W. Wang, E. Thomsen, D. Reed, B. Li, P. Balducci, M. Kintner-Meyer, and V. Sprinkle, *J. Power Sources*, **293**, 388 (2015).
8. R. M. Darling, K. G. Gallagher, J. A. Kowalski, and S. Ha, *Energy Environ. Sci.*, **7**, 3459 (2014).
9. C. Hagg and M. Skyllas-Kazacos, *J. Appl. Electrochem.*, **32**, 1063 (2002).
10. V. Haddadi-Asl and M. Kazacos, *J. Appl. Polym. Sci.*, **57**, 1455 (2003).
11. P. Qian, H. Zhang, J. Chen, Y. Wen, Q. Luo, and Z. Liu, *J. Power Sources*, **175**, 613 (2008).
12. E. Agar, C. R. Dennison, K. W. Knehr, and E. C. Kumbur, *J. Power Sources*, **225**, 89 (2013).
13. Q. H. Liu, G. M. Grim, A. B. Papandrew, A. Turhan, T. A. Zawodzinski, and M. M. Mench, *J. Electrochem. Soc.*, **159**, 1246 (2012).
14. M. P. Manahan, Q. H. Liu, M. L. Gross, and M. M. Mench, *J. Power Sources*, **222**, 498 (2013).
15. B. Li, M. Gu, Z. Nie, X. Wei, C. Wang, V. Sprenkle, and W. Wang, *Nano Lett.*, **14**, 158 (2013).
16. I. Mayrhuber, C. R. Dennison, V. Kalra, and E. C. Kumbur, *J. Power Sources*, **260**, 251 (2014).
17. J Zhang, L. Li, Z. Nie, B. Chen, M. Vijayakumar, S. Kim, W. Wang, B. Schwenzer, J. Liu, and Z. Yang, *J. Appl. Electrochem.*, **41**, 1215 (2011).
18. S. Kim, M. Vijayakumar, W. Wang, J. Zhang, B. Chen, Z. Nie, F. Chen, J. Hu, L. Li, and Z. Yang, *Phys. Chem. Chem. Phys.*, **13**, 18186 (2011).
19. M. Vijayakumar, L. Li, Z. Nie, Z. Yang, and J. Hu, *Phys. Chem. Chem. Phys.*, **14**, 10233 (2012).
20. W. N. Li, R. Zaffou, C. Sholvin, M. Perry, and Y. She, *ECS Trans.*, **53**, 93 (2013).
21. M. Vijayakumar, W. Wang, Z. Nie, V. Sprenkle, and J. Hu, *J. Power Sources*, **241**, 173 (2013).
22. K. W. Knehr, E. Agar, C. R. Dennison, A. R. Kalidindi, and E. C. Kumbur, *J. Electrochem. Soc.*, **159**, A1446 (2012).
23. A. Tang, J. Bao, and M. Skyllas-Kazacos, *J. Power Sources*, **196**, 10737 (2011).
24. M. Skyllas-Kazacos and L. Goh, *J. Membr. Sci.*, 399, 43 (2012).
25. R. Badrinarayanan, J. Zhao, K. J. Tseng, and M. Skyllas-Kazacos, *J. Power Sources*, **270**, 576 (2014).
26. E. Agar, K. W. Knehr, D. Chen, M. A. Hickner, and E. C. Kumbur, *Electrochim. Acta*, **98**, 66 (2013).
27. K. W. Knehr and E. C. Kumbur, *Electrochem. Commun.*, **23**, 76 (2012).
28. E. Agar, A. Benjamin, C. R. Dennison, D. Chen, M. A. Hickner, and E. C. Kumbur, *J. Power Sources*, **246**, 767 (2014).
29. A. Benjamin, E. Agar, C. R. Dennison, and E. C. Kumbur, *Electrochem. Commun.*, **35**, 42 (2013).
30. D. Bernardi and M. Verbrugge, *AIChE J.*, **37**, 1151 (1991).
31. J. Xi, Z. Wu, X. Teng, Y. Zhao, L. Chen, and X. Qui, *J. Mater. Chem.*, **18**, 1232 (2008).
32. G. Pourcelly, A. Lindheimer, and C. Gavach, *J. Electroanal. Chem.*, **305**, 97 (1991).
33. M. Verbrugge, *J. Electrochem. Soc.*, **137**, 893 (1990).
34. M. Verbrugge and R. Hill, *J. Electrochem. Soc.*, **137**, 886 (1990).
35. K. Kontturi, L. Murtomaki, and J. A. Manzanares, Ionic Transport Processes in Electrochemistry and Membrane Science, Oxford University Press, New York (2008).
36. J. Newman and K. E. Thomas-Alyea, *Electrochemical Systems*, 3rd edn, Wiley, New Jersey (2004).
37. P. Xu and B. Yu, *Adv. Water Resour.*, **31**, 74 (2008).
38. C. Sun, J. Chen, H. Zhang, X. Han, and Q. Luo, *J. Power Sources*, **195**, 890 (2010).
39. S. Slade, S. A. Campbell, T. R. Ralph, and F. C. Walsh, *J. Electrochem. Soc.*, **149**, A1556 (2002).
40. S. Kim, J. Yan, B. Schwenzer, J. Zhang, L. Li, J. Liu, Z. Yang, and M. A. Hickner, *Electrochem. Commun.*, **12**, 1650 (2010).